Journal of ELECTRONIC MATERIALS, Vol. 48, No. 7, 2019
https://doi.org/10.1007/s11664-019-07223-5

Preparation of a Homogeneous Li_3PO_4 Coating and Its Effect on the Electrochemical Properties of $LiNi_{0.8}Co_{0.15}Al_{0.05}O_2$

XINGWEN ZHANG,[1] GUOBIAO LIU,[2] SHAOMIN LI,[1] HANG DONG,[1,3] HAO LIU,[1] and JUN MEI[1,4]

1.—Chengdu Green Energy and Green Manufacturing Technology R&D Center, Chengdu Development Center of Science and Technology, China Academy of Engineering Physics, Chengdu 610200, China. 2.—Department of Materials Science, Sichuan Engineering Technical College, Deyang 618000, China. 3.—College of Materials Science and Engineering, Sichuan University, Chengdu 610064, China. 4.—e-mail: meijun16@126.com

A uniform nanocoating can substantially enhance the electrochemical properties of cathode materials. Herein, we report that a uniform $AlPO_4$ coating can be produced on the surface of $LiNi_{0.8}Co_{0.15}Al_{0.05}O_2$ (NCA) particles by a homogeneous precipitation method, which was confirmed by scanning electron microscopy and energy dispersive x-ray spectroscopy. After being heated, the $AlPO_4$ was converted to the Li_3PO_4 which was verified by x-ray diffraction. The heated $AlPO_4$ coated NCA demonstrated a substantially enhanced electrochemical performance. The capacity retention increased from 87.38% for bare NCA to 94.28% for the heated 1 wt.% $AlPO_4$ coated NCA sample. Moreover, the reversible capacity at 5 C increased from 80 mAh/g for bare NCA to 120 mAh/g for the heated 1 wt.% $AlPO_4$-coated NCA. In addition, improved thermal stability was also found. The start temperature of thermal runaway increased from 175.12°C for bare NCA to 200.32°C for the heated 1 wt.% $AlPO_4$-coated NCA.

Key words: Lithium batteries, $LiNi_{0.8}Co_{0.15}Al_{0.05}O_2$, $AlPO_4$, Li_3PO_4, homogenous coating, homogeneous precipitation method

INTRODUCTION

In the last decades, lithium-ion batteries (LIBs) have been used in portable electrical equipment since they were commercialized by Sony in 1991. In recent years, LIBs have been widely used in electric vehicles and hybrid electric vehicles.[1–6] To meet the demand for increasing mileage in electric vehicles, the energy density of LIBs must be substantially improved.[2] So far, using a cathode material possessing a high energy density is an effective way to improve the energy density for LIBs.[7] Due to its high energy density, $LiNi_{0.8}Co_{0.15}Al_{0.05}O_2$ (NCA) has attracted extensive attention.[8–10] Nevertheless, bare NCA usually demonstrates poor cycling stability and thermal stability because a large number of Ni^{4+} ions with strong oxidizability on the surface of NCA particles tend to react with the electrolyte.[11–14]

To improve the cycling and thermal stability, surface modification is widely used to decrease the Ni^{4+} content on the surface of NCA particles.[15] For instance, carbon materials,[16,17] oxides,[18,19] fluorides,[20] phosphates[21,22] and polymer coatings[15] have been prepared and confirmed to be helpful in improving the cycling and thermal stability of NCA. Among these coatings, the $AlPO_4$ coating has been widely investigated because it can be converted to Li_3PO_4 after being heated.[23] Li_3PO_4 acts as a portion of the solid electrolyte interface (SEI) film and facilitates the Li^+ transport across the SEI film,[24,25] which can promote the rate capability of NCA. Moreover, Li_3PO_4 can inhibit the corrosion of the electrolyte on the surface of the NCA particles.[26] Based on this mechanism, the cycling stability of the NCA can be increased. In addition, the Li_3PO_4 coating reduces the Ni^{4+} content on the surface of

(Received December 10, 2018; accepted April 12, 2019; published online April 24, 2019)

NCA particles and increases their thermal stability of NCA particles.[27]

Recently, uniform nanocoating layers on cathode materials have attracted attention because they improved the electrochemical properties of cathode materials.[28] A uniform Li_3PO_4 coating layer on the surface of $LiCoO_2$ was successfully fabricated by heating a uniform $AlPO_4$ coating prepared using a precipitation method by Yang et al.[29] These authors used $Al(NO_3)_3$ as well as $(NH_4)_2HPO_4$ as reactants and urea as a source of OH^-. The urea slowly releases OH^-, leading to a slow release of PO_4^{3-} from HPO_4^{2-}. The slow release of PO_4^{3-} contributes to the preparation of a uniform $AlPO_4$ coating. We repeated their work and found a shortcoming. Forming a uniform $AlPO_4$ coating on the surface of the particle required a large amount of urea. This is in accord with their work in which 0.5 g $CO(NH_2)_2$ was used to prepare 2.5 g $LiCoO_2$@$AlPO_4$. To our knowledge, it is difficult to reduce the required urea. To develop a more practical coating process, we tried another strategy of slowing the release of Al^{3+}.

In this article, based on the fact that $NaAlO_2$ can slowly release Al^{3+} and is inexpensive, we used $NaAlO_2$ as the reactant to form a uniform $AlPO_4$ coating on the surface of the NCA particles. After being heated, the uniform $AlPO_4$ coating film was converted to a uniform Li_3PO_4 coating. Furthermore, we investigated the influence of the Li_3PO_4 content on the electrochemical properties of the NCA.

EXPERIMENTAL

First, bare NCA powder was prepared by a high-temperature solid method. Five grams of $Ni_{0.842}Co_{0.158}(OH)_2$, 0.1443 g Al_2O_3 and 2.3773 g $LiOH{\cdot}H_2O$ (excess of 5%) were used as raw materials and were uniformly mixed based on the formula of $LiNi_{0.8}Co_{0.15}Al_{0.05}O_2$. Then, the mixture was calcined at 500°C for 5 h and 780°C for 16 h in an oxygen atmosphere. The obtained $LiNi_{0.8}Co_{0.15}Al_{0.05}O_2$ was designated as bare NCA.

The preparation process of 1 wt.% $AlPO_4$-coated NCA is illustrated in Fig. 1, where 0.0328 g $(NH_4)_2HPO_4$ was dissolved in 3 mL deionized water. The pH value of the $(NH_4)_2HPO_4$ solution was adjusted to 11 using NaOH. Then, 0.0204 g $NaAlO_2$ was dissolved into the $(NH_4)_2HPO_4$ solution. Afterwards, 3 g NCA was added to the $NaAlO_2$ and $(NH_4)_2HPO_4$ solution. Under intense stirring, a 0.1 mol/L H_2SO_4 solution was added dropwise into the $NaAlO_2$ and $(NH_4)_2HPO_4$ solution until the solution pH decreased to 9. Then, the $AlPO_4$-coated NCA was washed with deionized water and dried. The dried powder was mixed with 0.0417 g $LiOH{\cdot}H_2O$ based on the formula of Li_3PO_4. The mixture was calcined at 500°C for 5 h in an oxygen atmosphere. Four samples were prepared based on 1 wt.%, 2 wt.%, 3 wt.% and 20 wt.% $AlPO_4$ and were designated as heated 1 wt.% $AlPO_4$-coated NCA, heated 2 wt.% $AlPO_4$-coated NCA, heated 3 wt.% $AlPO_4$-coated NCA and heated 20 wt.% $AlPO_4$-coated NCA. Among these samples, the 20 wt.% $AlPO_4$-coated NCA was used to detect the crystalline structure of the coating material by x-ray diffraction since the 1 wt.%, 2 wt.% and 3 wt.% $AlPO_4$-coated NCAs did not show the presence of $AlPO_4$ in their x-ray diffraction (XRD) patterns.

The crystalline structure of the as-prepared materials was characterized with an x-ray diffractometer with Cu-Kα radiation at 40 kV. The morphology of the as-prepared materials was observed on a Hitachi S-5200 scanning electron microscope (SEM). The atomic ratio of Li/Ni/Co/Al in a sample was confirmed by inductively coupled plasma spectrometry. The content of PO_4^{3-} was verified by ion chromatography. The elemental distributions of Ni, Co, Al and P were observed with an energy-dispersive x-ray (EDX) spectrometer. The specific crystallographic planes of the samples were observed using

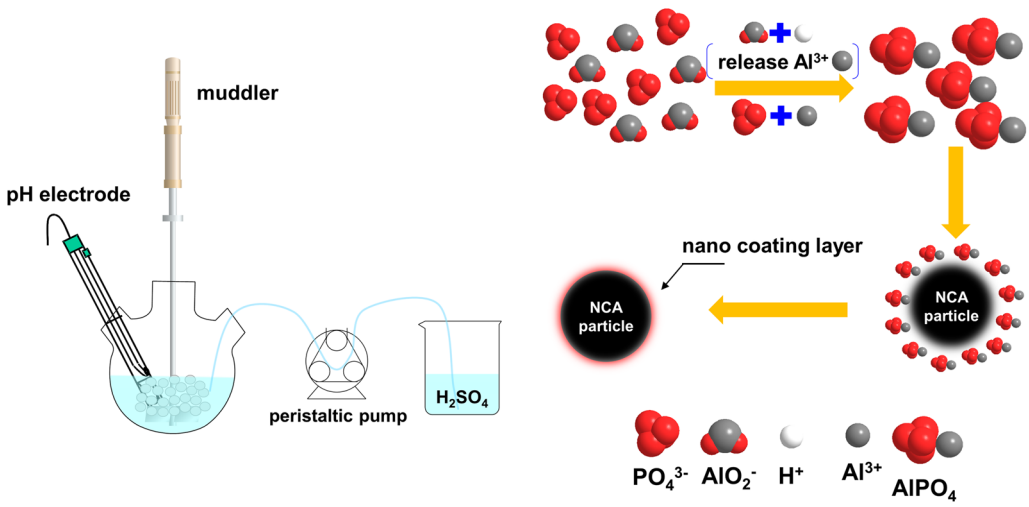

Fig. 1. Schematic picture for preparing $AlPO_4$-coated NCA.

an FEI TecnaiG2 high-resolution transmission electron microscope (HR-TEM). The valence states of Li, Ni, Co, Al, O and P were investigated using x-ray photoelectron spectrometry (XPS). Thermal stabilities of the bare and heated $AlPO_4$-coated NCAs were studied using differential scanning calorimetry (DSC).

The electrochemical performance was tested using coin cells. The details of constructing the cells and assessing the electrochemical properties were described in previous studies.[30,31]

RESULTS AND DISCUSSION

Figure 2 shows XRD patterns and SEM images of bare and $AlPO_4$-coated NCAs. As shown in Fig. 2a, the bare, 1 wt.%, 2 wt.% and 3 wt.% $AlPO_4$-coated NCAs had similar XRD patterns. All peaks were indexed to a layered α-$NaFeO_2$ structure with a $R\bar{3}m$ space group. The 20 wt.% $AlPO_4$-coated NCA sample had a slightly different XRD pattern from the other samples. The main peaks were indexed to a layered α-$NaFeO_2$ structure,[18] and the weak peak at 15.9° was indexed to a triclinic $AlPO_4$ (JCPDS: 79-2246) structure. The weak peak indicated that

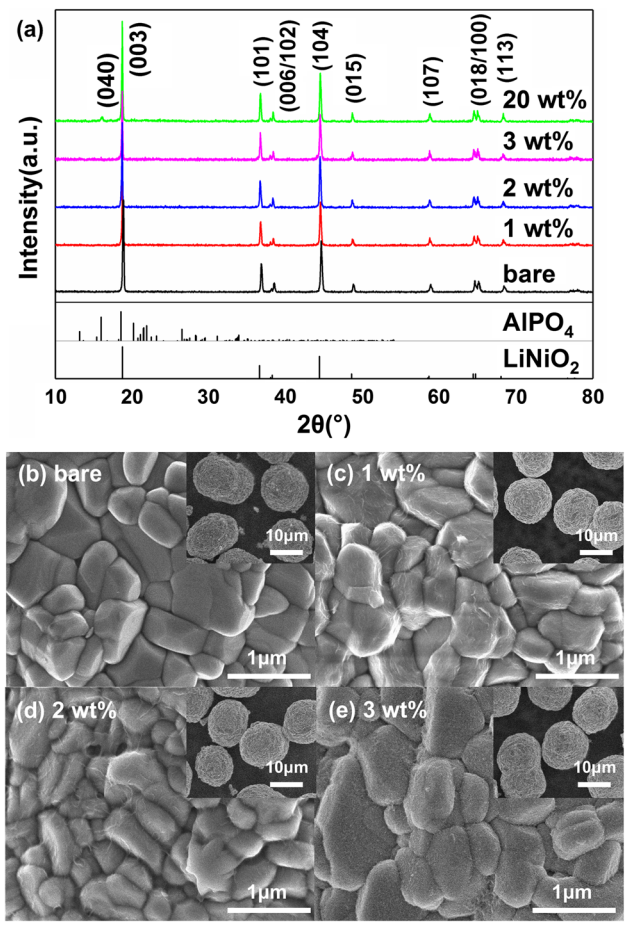

Fig. 2. XRD patterns (a) and SEM images (b, c, d, e) of bare and $AlPO_4$-coated NCA.

the $AlPO_4$ had a poor crystalline structure. As shown in Fig. 2b, c, d, and e, the bare, 1 wt.%, 2 wt.% and 3 wt.% $AlPO_4$-coated NCAs, respectively, had similar morphologies in the low-resolution images. However, the bare NCA had a smooth surface in the high-resolution images. The 1 wt.%, 2 wt.% and 3 wt.% $AlPO_4$-coated NCAs had a relatively uniform coating on the surface of the primary particles. The atomic ratio of Li/Ni/Co/Al was obtained to confirm the chemical compositions of the samples. As listed in supplementary Table S1, the calculated atomic ratio of the bare NCA was close to that of the chemical formula for $LiNi_{0.8}Co_{0.15}Al_{0.05}O_2$. Moreover, the weight percentage of PO_4^{3-} was examined. The calculated weight percentages of $AlPO_4$ for the three samples were close to 1 wt.%, 2 wt.% and 3 wt.%. Based on the analysis of the XRD pattern for the 20 wt.% $AlPO_4$-coated NCA, the change in the Li/Ni/Co/Al atomic ratio and the weight percentage of PO_4^{3-}, the uniform coating observed in the SEM images on the 1 wt.%, 2 wt.% and 3 wt.% $AlPO_4$-coated NCAs should be $AlPO_4$. The mechanism to form a uniform $AlPO_4$ coating can be described as follows. When the pH value was 11, PO_4^{3-} and AlO_2^- existed stably in the $NaAlO_2$ and $(NH_4)_2HPO_4$ solution. When the pH value decreased by slowly adding H_2SO_4 solution, AlO_2^- slowly released Al^{3+}. The Al^{3+} reacted with the PO_4^{3-}. The specific chemical reaction is as follows.

$$AlO_2^- + 4H^+ + PO_4^{3-} \rightarrow AlPO_4 \downarrow + 2H_2O.$$

Due to the slow release of Al^{3+}, $AlPO_4$ uniformly covered the surface of the cathode materials.

Figure 3 shows the EDX mapping, TEM and HR-TEM images of the 1 wt.% $AlPO_4$-coated NCA. As illustrated in Fig. 3a, Ni, Co, Al and P are uniformly dispersed on the surface of the NCA spherical particle, which is in accord with the SEM image. As shown in Fig. 3b (a low-resolution TEM image), an 18 nm thick coating layer marked by a red line is clearly present at the edge of the primary particle. As shown in Fig. 3c (a high-resolution TEM image), clear lattice fringes can be observed in the middle of the particle, while no clear lattice fringes can be detected in the coating layer marked by the red line, indicating that the $AlPO_4$ coating had poor crystallinity. This result agrees with the analysis of the XRD pattern of 20 wt.% $AlPO_4$-coated NCA.

Figure 4 exhibits XRD patterns along with SEM images of the heated $AlPO_4$-coated NCAs. As illustrated in Fig. 4a and Fig. 2a, the XRD patterns of 1 wt.%, 2 wt.% and 3 wt.% $AlPO_4$-coated NCAs before and after heating were very similar, and no impurity was detected. However, weak peaks at 22.3° and 23.1° were detected in the XRD pattern of heated 20 wt.% $AlPO_4$-coated NCA. These weak peaks can be indexed to the orthorhombic Li_3PO_4 structure, indicating that $AlPO_4$ is converted to Li_3PO_4 after being heated. This result is in accord with a previous report that Li_3PO_4, rather than

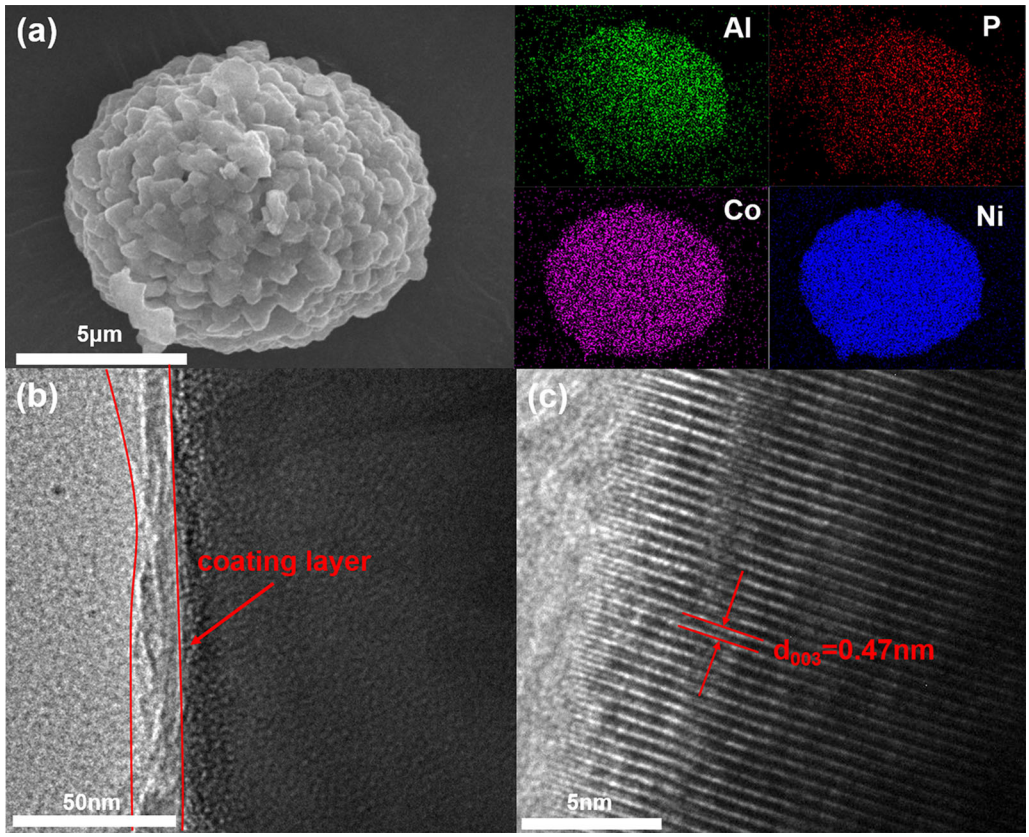

Fig. 3. EDX mapping (a), TEM (b) and HR-TEM (c) images of 1 wt.% $AlPO_4$-coated (Color figure online).

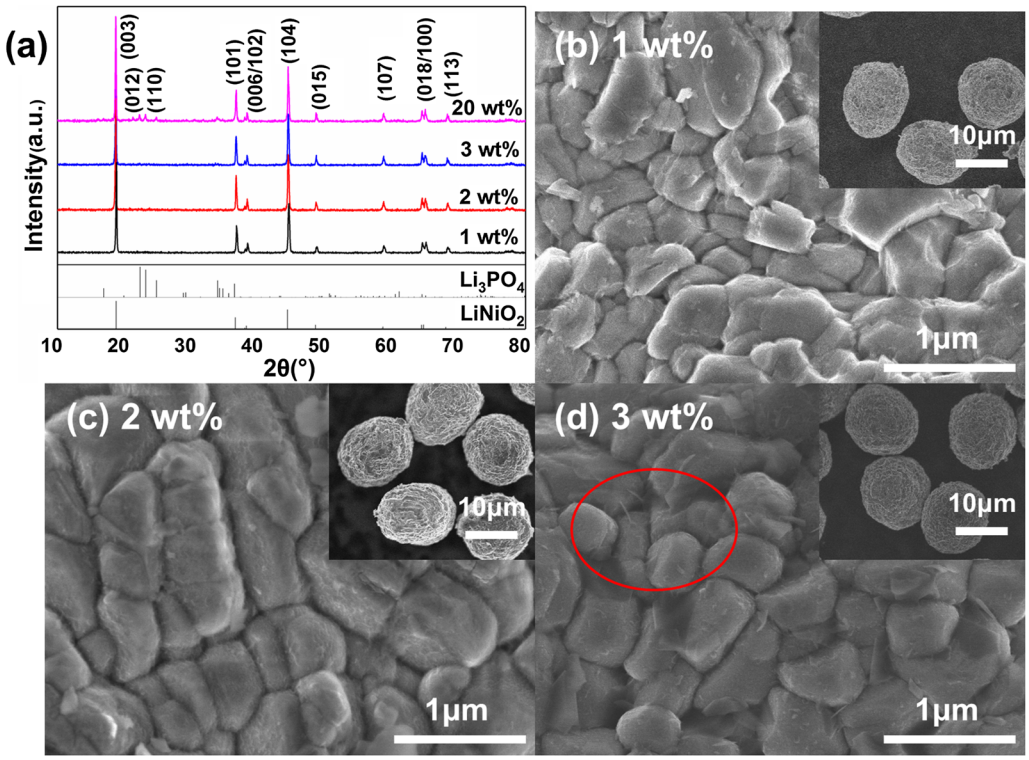

Fig. 4. XRD patterns (a) and SEM images (b, c, d) of heated $AlPO_4$-coated NCA.

$AlPO_4$ or $LiAlO_2$, was present on the surface of $LiCoO_2$ particles and other cathode materials.[32–34] Additional evidence to support this conclusion is illustrated by the analysis of XPS spectra.

As shown in Fig. 4b, c, and d, the clear $AlPO_4$ coating shown in Fig. 2c, d, and e disappears. Some nanoplates are observed in the SEM image of heated 3 wt.% $AlPO_4$-coated NCA. The reason for this morphology can be explained as follows. After being heated, the $AlPO_4$ coating layer was converted to a Li_3PO_4 coating layer. The Li_3PO_4 coating adhered tightly to the NCA particles when the $AlPO_4$ content was 1 wt.% and 2 wt.%. Excess Li_3PO_4 covered the surface of the Li_3PO_4 coating in the form of nanoplates when the $AlPO_4$ content was 3 wt.%.

To compare the change in surface properties between bare NCA and heated $AlPO_4$-coated samples, XPS spectra were collected to detect the valence state of the elements. Figure 5 presents the XPS spectra of bare and heated 1 wt.% $AlPO_4$-coated NCA. As shown in Fig. 5a, the Li 1 s XPS spectra for both samples were similar. The peak at 55.0 eV was attributed to Li^+.[35] In Fig. 5b, the Ni 2*p* XPS spectra for both samples were similar. The Ni $2p_{3/2}$ peaks at 855.5 eV and 861.2 eV indicated the existence of Ni^{2+} and Ni^{3+}, respectively.[36,37] In Fig. 5c, the Co 2*p* XPS spectra for both samples were also similar. The Co $2p_{3/2}$ peak at 780.2 eV and Co $2p_{1/2}$ peak at 795.0 eV indicated that Co^{3+} existed in both samples.[35] In Fig. 5d, the Al 2*p* XPS spectra for both samples were different. The peak at 73.7 eV for the heated 1 wt.% $AlPO_4$-coated NCA was intense, while the peak for bare NCA was weak. The reason for this difference is that the $LiAlO_2$ phase was formed, and a portion of Al^{3+} was

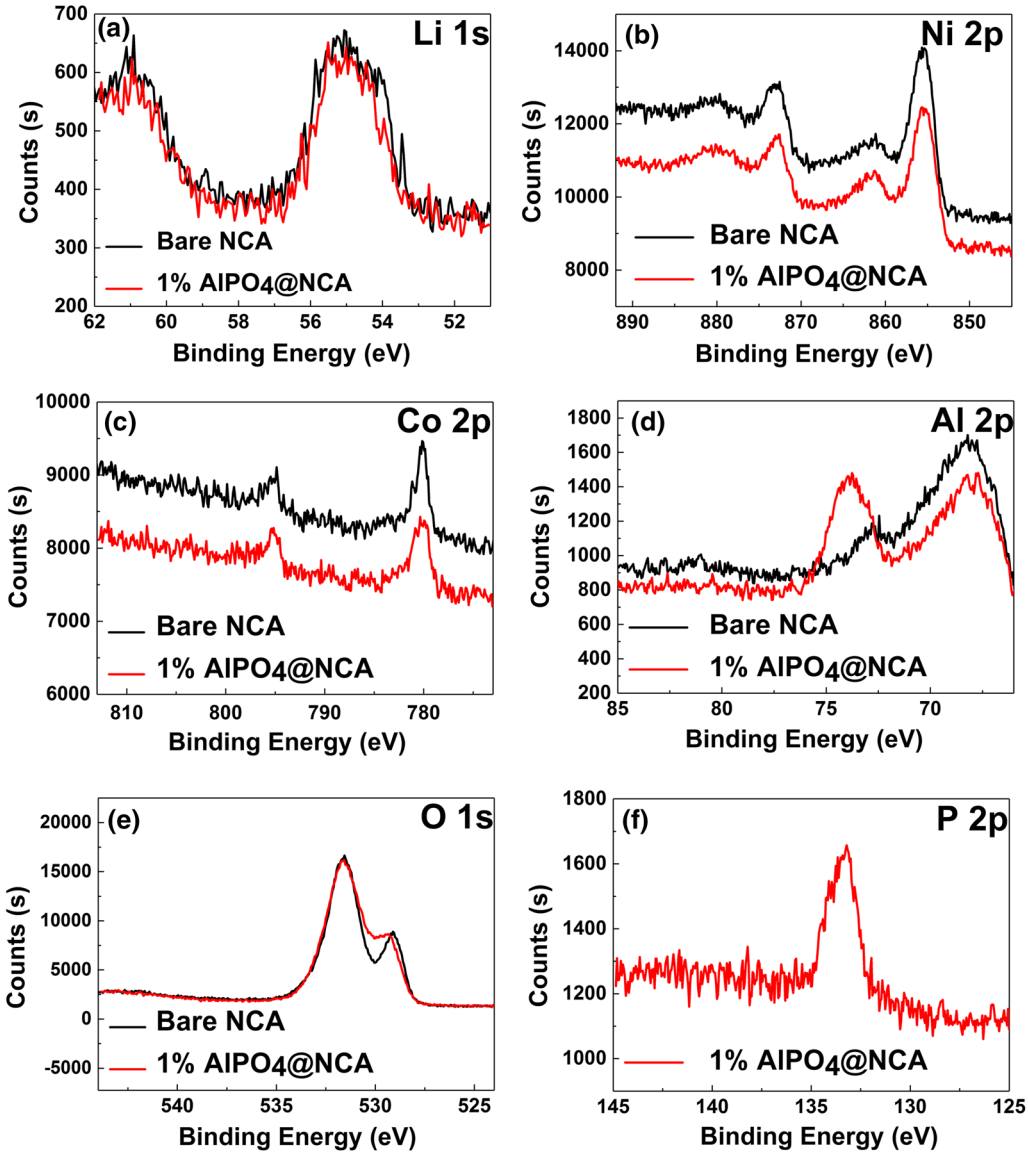

Fig. 5. XPS spectra of bare and heated 1 wt.% $AlPO_4$-coated NCA: (a) Li1s, (b) Ni 2*p*, (c) Co 2*p*, (d) Al 2*p*, (e) O1s, (f) P 2*p*.

introduced into the NCA matrix. Additionally, the content of Al on the surface after coating was higher than that in the original sample. The peak at 73.7 eV was attributed to Al^{3+} in $LiAlO_2$ or Al^{3+} introduced into the NCA matrix.[32,33] The O 1 s XPS spectra for both samples were also different. The peak at 529.5 eV for heated 1 wt.% $AlPO_4$-coated NCA was weak, while the peak for bare NCA was strong. The intensity difference of the peak at 529.5 eV for both samples was ascribed to the Al^{3+} introduced into the NCA matrix based on a previous report that the peak at 529.5 eV for Al-substituted $LiCoO_2$ was weak, while the peak for bare $LiCoO_2$ was strong.[32–34] This result agrees with the XRD analysis that no $LiAlO_2$ was observed in the XRD pattern of the heated 20 wt.% $AlPO_4$-coated NCA. As shown in Fig. 5f, the P 2*p* XPS peak at 133.2 eV is attributed to the P^{5+} in Li_3PO_4 rather than $AlPO_4$ since the P 2*p* XPS peak of $AlPO_4$ is 134.4 eV.[32–34] This result is also in accord with the XRD analysis that no $AlPO_4$ was observed in the XRD pattern of the heated 20 wt.% $AlPO_4$-coated NCA. The combined XRD and XPS results indicated that the $AlPO_4$ on the surface of the heated 1 wt.% $AlPO_4$-coated NCA was converted to Li_3PO_4 and that Al^{3+} was introduced into the NCA matrix.

Figure 6 shows EDX maps, TEM and HR-TEM images of heated 1 wt.% $AlPO_4$-coated NCA. As illustrated in Fig. 6a, Ni, Co, Al and P were still uniformly dispersed on the surface of the NCA particle. As illustrated in Fig. 6b (a low-resolution TEM image), a 10 nm thick coating layer marked with a red line was present at the edge of the primary particle. The EDX maps and low-resolution TEM image indicate that the Li_3PO_4 coating adhered tightly to the NCA particle when the $AlPO_4$ content was 1 wt.%. As shown in Fig. 6c (a high-resolution TEM image), clear lattice fringes can be observed in the middle of the particle and in the coating layer marked with a red line. The interplanar spacing of the lattice fringes in the middle of the particle was 0.47 nm, while that in the coating layer was 0.21 nm. The 0.47 nm interplanar spacing indicated that the lattice fringes belong to the layered NCA.[12] The 0.21 nm interplanar spacing indicated that the [212] lattice fringes belong to the orthorhombic Li_3PO_4.[38] The result is in accord with the XRD patterns in Fig. 5a.

Figure 7a shows the initial charge and discharge curves of bare and heated 1 wt.%, 2 wt.%, 3 wt.% $AlPO_4$-coated NCAs at 0.1 C in a voltage range of 2.8-4.3 V. The profiles for bare and coated NCAs are similar, which indicates that the heated $AlPO_4$ coating did not change the charge and discharge mechanism of NCA. Table S2 (see supplementary Table S2) exhibits the specific data of charge capacity, discharge capacity and coulombic efficiency. When the percentage content of $AlPO_4$ was

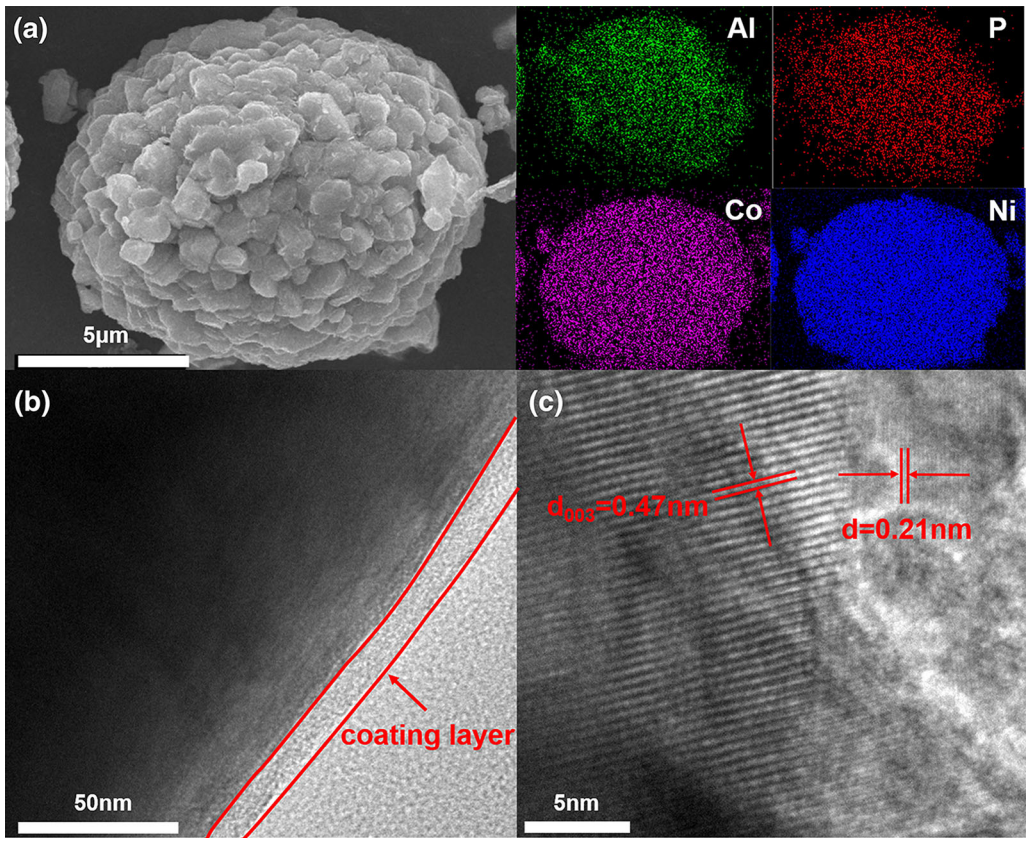

Fig. 6. EDX mapping (a), TEM (b) and HR-TEM (c) images of heated 1 wt.% $AlPO_4$-coated NCA.

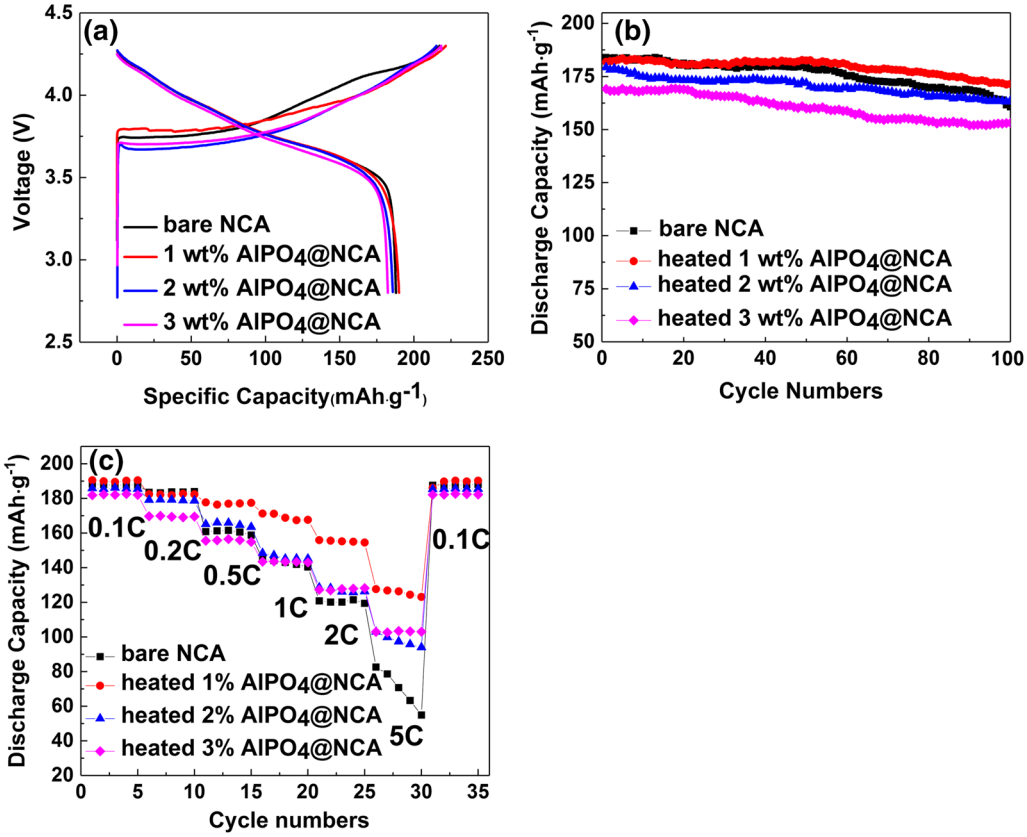

Fig. 7. Electrochemical performances of bare and heated $AlPO_4$-coated NCA: (a) initial charge–discharge curves at 0.1 C, (b) cycling stability at 0.2 C, (c) rate capability.

1%, the reversible capacity increased slightly, and the coulombic efficiency remained almost unchanged. When the percentage content of $AlPO_4$ increased to 3%, the reversible capacity and coulombic efficiency decreased. The reason is that some nano-plates on the surface of heated 3 wt.% $AlPO_4$-coated NCA cause a side reaction with the electrolyte. Figure 7b shows the cycling performance of bare and heated 1 wt.%, 2 wt.%, 3 wt.% $AlPO_4$-coated NCA at 0.2 C. Table S3 (see supplementary Table S3) lists the specific data of the first and 100th discharge capacities as well as capacity retentions. As shown in supplementary Table S3, $AlPO_4$-coated NCA exhibited an improved cycling stability. Heated 1 wt.% $AlPO_4$-coated NCA had the highest capacity retention of 94.28% after 100 cycles, while the bare NCA had the lowest capacity retention of 86.47%. As illustrated in previous studies, an appropriate coating amount of $AlPO_4$ or Li_3PO_4 can substantially improve the cycling stability of the cathode material. An excess coating amount usually has a minor positive impact or a negative impact on the cycling stability of the cathode material. The reason for this behavior may be as follows. The coating restrained the corrosion of the electrolyte, leading to an improvement in the cycling stability. An appropriate coating amount reduced the resistance of the SEI film (R_{SEI}) as well as the charge transfer resistance (R_{ct}), which substantially improved the cycling stability. An excess coating amount increased the R_{SEI} as well as the R_{ct}, which decreased the cycling stability. The resistance data for the as-prepared samples are provided in the following section. Figure 7c shows the rate capability of bare and heated 1 wt.%, 2 wt.%, 3 wt.% $AlPO_4$-coated NCAs. Heated $AlPO_4$-coated NCAs had an improved rate capability. The heated 1 wt.% $AlPO_4$-coated NCA had the best rate capability of the samples considered in this study. Overall, the heated $AlPO_4$ coating helped to improve the electrochemical properties of NCAs, which is in agreement with the conclusions in previous studies.[21,35,39–42]

To probe the influence of the heated $AlPO_4$ layer on the resistance of the NCA electrode, electrochemical impedance spectra (EIS) were collected on the cells after the first and 100th cycles at 0.2 C. Nyquist plots of the bare and heated $AlPO_4$-coated NCA and an equivalent circuit model are presented in Fig. 8. Each Nyquist plot had two semicircles that were fit using the equivalent circuit at the bottom of Fig. 8. In the Nyquist plot, the point at the highest frequency represents the ohmic resistance (R_e). The first semicircle in the high frequency region denotes R_{SEI}. The second semicircle in the middle frequency region denotes R_{ct}.[43–46] Table S4

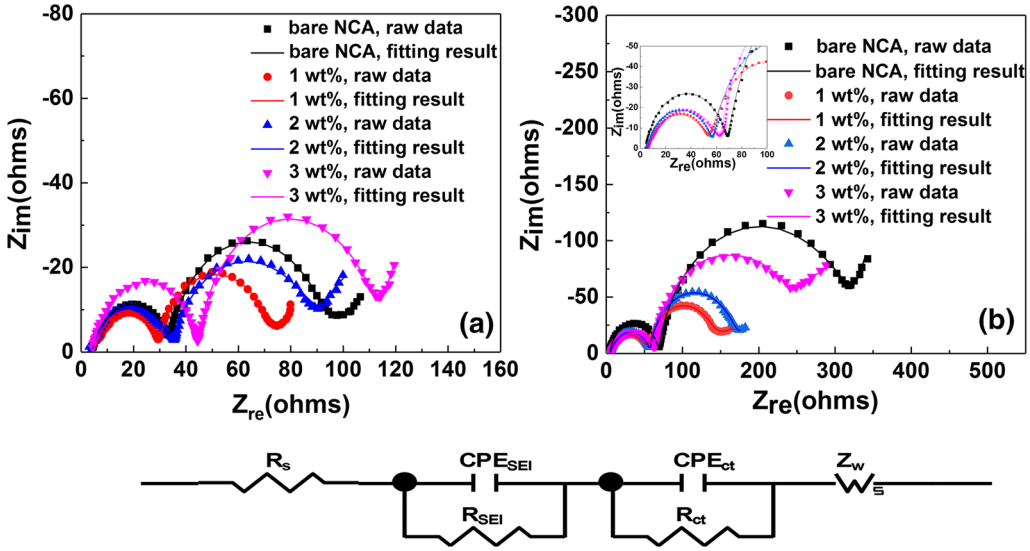

Fig. 8. Nyquist plots of bare and heated $AlPO_4$-coated NCA: (a) after initial cycle at 0.2 C, (b) after 100 cycles at 0.2 C (the inset: magnified images of the high frequency region). An equivalent circuit model for fitting.

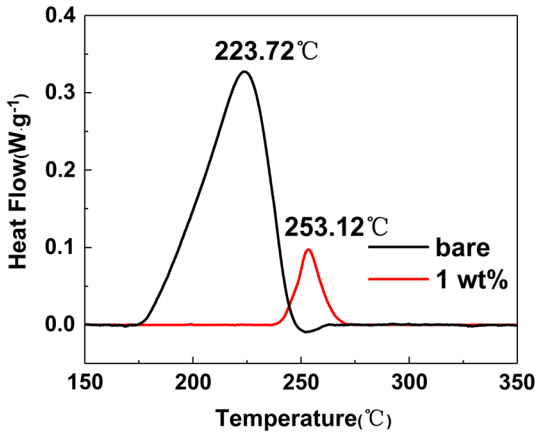

Fig. 9. DSC curves of bare and heated 1wt.% $AlPO_4$-coated NCA.

(see supplementary Table S4) provides the fitted impendence values. Table S4 shows that the total resistance value of heated $AlPO_4$-coated NCA increased slowly after 100 cycles. However, the total resistance value of the bare NCA increased quickly. The heated $AlPO_4$ coating reduced the resistance increase, which agrees with the improved cycling performance.

To probe the influence of the heated $AlPO_4$ layer on the thermal stability of the NCA, DSC curves of bare NCA and heated 1 wt.% $AlPO_4$-coated NCA were obtained. As shown in Fig. 9, the exothermic peak for heated 1 wt.% $AlPO_4$-coated NCA occurred at 253.12°C, while the exothermic peak for bare NCA occurred at 223.72°C. After being coated with the heated $AlPO_4$, the NCA had a higher start temperature for thermal runaway. Furthermore, the heat release from the exothermic reaction for the heated 1 wt.% $AlPO_4$-coated NCA was 1.29 J/g, while the heat release for bare NCA was 11.65 J/g. As reported in previous studies,[21,35,39–42] two factors determine the start temperature of thermal runaway. First, oxygen released from the lattice can react with the organic solvent of the electrolyte, leading to heat generation. Second, Ni^{4+} ions with a strong oxidizability on the surface of NCA particles can also react with the organic solvent of the electrolyte, resulting in heat generation. The heated $AlPO_4$ coating reduces the Ni^{4+} content on the surface of NCA particles, restraining the exothermic reaction of the cathode with the electrolyte. Therefore, the heated $AlPO_4$-coated NCA had a higher start temperature for thermal runaway and a lower heat release than those of the bare NCA.

CONCLUSION

In this study, a uniform $AlPO_4$ coating on the surface of NCA particles was produced by a homogeneous precipitation method using $NaAlO_2$ as a source of Al^{3+}. After being heated, the uniform $AlPO_4$ coating layer was converted to a uniform Li_3PO_4 coating layer. Al^{3+} in $AlPO_4$ was introduced into the NCA matrix. The heated $AlPO_4$ coating improved the electrochemical performance and thermal stability of the NCA. In addition, the homogeneous precipitation method was straightforward.

ACKNOWLEDGMENTS

The research was financially supported by the Sichuan Provincial Key Technology R&D Program (2016GZ0299).

ELECTRONIC SUPPLEMENTARY MATERIAL

The online version of this article (https://doi.org/10.1007/s11664-019-07223-5) contains supplementary material, which is available to authorized users.

REFERENCES

1. J.W. Choi and D. Aurbach, *Nat. Rev. Mater.* 1, 16013 (2016).
2. J.B. Goodenough and Y. Kim, *Chem. Mater.* 22, 587 (2010).
3. C.P. Grey and J.M. Tarascon, *Nat. Mater.* 16, 45 (2016).
4. P.Y. Hou, L.Q. Zhang, and X.P. Gao, *J. Mater. Chem. A* 2, 17130 (2014).
5. P.K. Nayak, E. Levi, J. Grinblat, M. Levi, B. Markovsky, N. Munichandraiah, Y.K. Sun, and D. Aurbach, *Chemsuschem* 9, 2404 (2016).
6. N. Nitta, F. Wu, J.T. Lee, and G. Yushin, *Mater. Today* 18, 252 (2015).
7. R. Robert, C. Villevieille, and P. Novák, *J. Mater. Chem. A* 2, 8589 (2014).
8. J. Kim, H. Lee, H. Cha, M. Yoon, M. Park, and J. Cho, *Adv. Energy Mater.* 8, 1870023 (2018).
9. S.-T. Myung, F. Maglia, K.-J. Park, C.S. Yoon, P. Lamp, S.-J. Kim, and Y.-K. Sun, *ACS Energy Lett.* 2, 196 (2016).
10. Y. Xia, J. Zheng, C. Wang, and M. Gu, *Nano Energy* 49, 434 (2018).
11. E. Cho, S.W. Seo, and K. Min, *ACS Appl. Mater. Interfaces* 9, 33257 (2017).
12. P. Hou, H. Zhang, X. Deng, X. Xu, and L. Zhang, *ACS Appl. Mater. Interfaces* 9, 29643 (2017).
13. E. Jo, S. Hwang, S.M. Kim, and W. Chang, *Chem. Mater.* 29, 2708 (2017).
14. F. Schipper, E.M. Erickson, C. Erk, J.-Y. Shin, F.F. Chesneau, and D. Aurbach, *J. Electrochem. Soc.* 164, A6220 (2016).
15. T. Chen, X. Li, H. Wang, X. Yan, L. Wang, B. Deng, W. Ge, and M. Qu, *J. Power Sour.* 374, 1 (2018).
16. Y.-M. Chung, S.-H. Ryu, J.-H. Ju, Y.-R. Bak, M.-J. Hwang, K.-W. Kim, K.-K. Cho, and K.-S. Ryu, *Bull. Korean Chem. Soc.* 31, 2304 (2010).
17. S. Yoon, K.-N. Jung, S.-H. Yeon, C.S. Jin, and K.-H. Shin, *J. Electroanal. Chem.* 683, 88 (2012).
18. G. Dai, M. Yu, F. Shen, J. Cao, L. Ni, Y. Chen, Y. Tang, and Y. Chen, *Ionics* 22, 2021 (2016).
19. B. Han, B. Key, S.H. Lapidus, J.C. Garcia, H. Iddir, J.T. Vaughey, and F. Dogan, *ACS Appl. Mater. Interfaces* 9, 41291 (2017).
20. H.B. Kim, B.C. Park, S.T. Myung, K. Amine, J. Prakash, and Y.K. Sun, *J. Power Sour* 179, 347 (2008).
21. R. Qi, J.-L. Shi, X.-D. Zhang, X.-X. Zeng, Y.-X. Yin, J. Xu, L. Chen, W.-G. Fu, Y.-G. Guo, and L.-J. Wan, *Sci China Chem* 60, 1230 (2017).
22. G. Wu and Y. Zhou, *J. Energy Chem.* 28, 151 (2018).
23. K. Min, S.W. Seo, B. Choi, K. Park, and E. Cho, *ACS Appl. Mater. Interfaces* 9, 17822 (2017).
24. S. Chen, T. He, Y. Su, Y. Lu, L. Bao, L. Chen, Q. Zhang, J. Wang, R. Chen, and F. Wu, *ACS Appl. Mater. Interfaces* 9, 29732 (2017).
25. J. Cho, Y.W. Kim, B. Kim, J.G. Lee, and B. Park, *Angew. Chem. Int. Ed. Engl.* 42, 1618 (2003).
26. D. Chen, F. Zheng, L. Li, M. Chen, X. Zhong, W. Li, and L. Lu, *J. Power Sour.* 341, 147 (2017).
27. Z.-F. Tang, R. Wu, P.-F. Huang, Q.-S. Wang, and C.-H. Chen, *J. Alloys Compd.* 693, 1157 (2017).
28. P. Hou, H. Zhang, Z. Zi, L. Zhang, and X. Xu, *J. Mater. Chem. A* 5, 4254 (2017).
29. F.L. Yang, W. Zhang, Z.X. Chi, F.Q. Cheng, J.T. Chen, A.M. Cao, and L.J. Wan, *Chem. Commun. (Camb.)* 51, 2943 (2015).
30. H. Dong, S. Li, H. Liu, J. Mei, H. Liu, and G. Liu, *Ionics* 25, 827 (2019).
31. Y. Zhou, Y. Wang, S. Li, J. Mei, H. Liu, H. Liu, and G. Liu, *J. Alloys Compd.* 695, 2951 (2017).
32. A.T.M. Appapillai, A.N. Mansour, J. Cho, and Y. Shao-Horn, *Chem. Mater.* 19, 10 (2007).
33. F. Wu, X. Zhang, T. Zhao, L. Li, M. Xie, and R. Chen, *ACS Appl. Mater. Interfaces* 7, 3773 (2015).
34. Y. Wu, A.V. Murugan, and A. Manthiram, *J. Electrochem. Soc.* 155, A635 (2008).
35. G.-R. Hu, X.-R. Deng, Z.-D. Peng, and K. Du, *Electrochim. Acta* 53, 2567 (2008).
36. Z.W. Lebens-Higgins, S. Sallis, N.V. Faenza, F. Badway, N. Pereira, D.M. Halat, M. Wahila, C. Schlueter, T.-L. Lee, W. Yang, C.P. Grey, G.G. Amatucci, and L.F.J. Piper, *Chem. Mater.* 30, 958 (2018).
37. L. Liang, X. Sun, C. Wu, L. Hou, J. Sun, X. Zhang, and C. Yuan, *ACS Appl. Mater. Interfaces* 10, 5498 (2018).
38. Y.K. Hu, J.X. Ren, Q.L. Wei, X.D. Guo, Y. Tang, B.H. Zhong, and H. Liu, *Acta Phys. Chim. Sin.* 30, 75 (2014).
39. J. Cho, T.-G. Kim, C. Kim, J.-G. Lee, Y.-W. Kim, and B. Park, *J. Power Sour.* 146, 58 (2005).
40. L. Li, Y. Cao, H. Zheng, and C. Feng, *J. Mater. Sci. Mater. Electron.* 28, 1925 (2016).
41. X. Ma, C. Wang, X. Han, and J. Sun, *J. Alloys Compd.* 453, 352 (2008).
42. Y. Zeng and J. He, *J. Power Sour.* 189, 519 (2009).
43. Y. Chen, K. Xie, C. Zheng, Z. Ma, and Z. Chen, *ACS Appl. Mater. Interfaces* 6, 16888 (2014).
44. B. Qiu, J. Wang, Y. Xia, Z. Wei, S. Han, and Z. Liu, *ACS Appl. Mater. Interfaces* 6, 9185 (2014).
45. L. Xiong, Y. Xu, T. Tao, and J.B. Goodenough, *J. Power Sour.* 199, 214 (2012).
46. J.M. Zheng, X.B. Wu, and Y. Yang, *Electrochim. Acta* 56, 3071 (2011).